Article

Dynamic Response Analysis and Positioning Performance Evaluation of an Arctic Floating Platform Based on the Mooring-Assisted Dynamic Positioning System

Yingbin Gu [1], Zhenju Chuang [2,*], Aobo Zhang [2,*], Ankang Hu [2] and Shunying Ji [3]

1   China National Nuclear Power Co., Ltd., Beijing 100822, China
2   Naval Architecture and Ocean Engineering College, Dalian Maritime University, Dalian 116026, China
3   State Key Laboratory of Structural Analysis for Industrial Equipment, Dalian University of Technology, Dalian 116024, China
*   Correspondence: zhenjuchuang@dlmu.edu.cn (Z.C.); zhangaobo@dlmu.edu.cn (A.Z.)

Abstract: The Arctic region is rich in oil and gas resources, but exploitation of resources there is always facing great challenge. Floating offshore platform is considered as a practical choice for oil and gas exploration in the Arctic deep water regions. One of the key technologies is positioning system design under harsh arctic sea loads. In this paper, a comprehensive design of the positioning system is investigated. A coupled numerical model composed of a mooring-assisted dynamic positioning system and the Kulluk platform is established. 16 different positioning combination forms are selected and investigated. The positioning capability of the coupled system is evaluated by analyzing the platform motion response under different environmental loads, including wave, level ice, and broken ice floes. Wave load is calculated using potential flow theory. Computation of ice load is compared with the finite element method (FEM) and discrete element method (DEM). The dynamic analysis of the mooring system is carried out by using the slender finite element method. The control system of dynamic positioning adopts proportional-integral-derivative (PID) control methodology. It is found that a better positioning system design can reduce the offset by more than 50%, including surge, sway and yaw motion. The results of this study will provide a good reference for the positioning system design of an arctic floating production platform.

Keywords: mooring-assisted dynamic positioning system; ice load; Arctic oil and gas resources; floating structure; Arctic technology

1. Introduction

A large number of un-developed oil and gas resources exist in the Arctic region, which has been widely concerned by various countries. The Arctic region is not only of great energy potential but also of strategic importance [1]. Henderson and Loe [2] provide an updated overview of offshore oil and gas developments in the Arctic and to discuss the potential for large-scale development of the region as a petroleum province over the next 20–30 years. Global warming, which has reduced the ice-covered area in the Arctic region, has also opened up the possibility of shipping routes. It has become a hot topic in the academic community how to conduct offshore operations in the Arctic region for offshore platforms used for the exploration and exploitation of resources. In recent years, scientific and technological progress has been made in the field of offshore floating platforms, including the development of traditional oil and gas resources and the development of new energy sources such as wind and wave energy [3,4]. However, there is not much research on floating offshore platforms operating in the Arctic environmental conditions. Amaechi et al. [5] gives a comprehensive review of different floating offshore platforms and introduces their applications in oil exploration and production. From the mid 1970s to the early 1990s, the "Kulluk" [6] were used fordrilling operations in Beaufort

Sea. It operated in a much wider and more difficult range of pack ice conditions than other platforms. The "ice performance information" was systematically obtained during its operations. Therefore, the Kulluk's experience provides the best source of data for most considerations related to moored vessel stationkeeping operations in various pack ice conditions. Wright [6] analyzed the field data of motion response and mooring system force of the Kulluk under the mooring state under the ice condition, and compared it with the results of model test. Zhou et al. [7] described a two-dimensional numerical model for the interaction between drifting level ice and the Kulluk platform. They studied the effects of ice thickness, ice drift speed, and global mooring stiffness on mooring forces and responses of the moored vessel. Kong et al. [8] established a high-performance discrete element method (DEM) for ice modeling based on the CUDA-C parallel processing technique. The Voronoi algorithm was used to generate the ice fragmentation field during the platform's operation. The moored structure's overall ice load under the continuous action of ice was calculated, and the numerical results were validated with the Kulluk's field test results. Jang and Kim [9] simulated the ice load on the Kulluk-shaped arctic floating platform using a self-programming method. Considering various uncertainties of model-ice properties and randomness/non-repeatability of fragmentation, the mean and maximum values of the ice load on the platform are obtained, which are close to the experimental results. Zhang and Chuang et al. [10] analyzed the dynamic response of a semi-submersible offshore platform under wave and ice loads by using the fully coupled time-domain method, and then optimized the platform structure.

Positioning system plays a very important role for floating platform system design. Traditional positioning methods include mooring positioning and dynamic positioning. The accuracy of the mooring system will decrease obviously in the harsh environment. Dynamic positioning system has high energy consumption, complex equipment, and high cost. Therefore, the mooring-assisted dynamic positioning system has become the main design scheme in ocean engineering field. It has the advantages of both mooring system and dynamic positioning, which effectively improves the safety of offshore operations. Sargent and Morgan [11] first introduced mooring-assisted dynamic positioning system. The research showed that the mooring-assisted dynamic positioning system could improve the positioning accuracy of floating structures and reduce the power consumption of dynamic positioning compared with the single positioning method. At the same time, the preliminary design of this positioning system was carried out. Strand [12] took the restoring force of the mooring system into consideration in the design of the dynamic positioning system. In this study, a mathematical model of the mooring-assisted dynamic positioning system was proposed, which further improved the positioning accuracy of floating structures. Aamo et al. [13] proposed a dynamic tension control method to change the restoring force of the mooring system by changing the length of the catenary. Through this method, the total restoring force could be provided to the maximum extent, and the rest was provided by the thrusters of the dynamic positioning system. A fault-tolerant control method for the mooring-assisted dynamic positioning system of a FPSO was proposed by Fang and Blanke [14]. A new position recovery algorithm was used to ensure the safety of the mooring system. The performance of the algorithm was verified by high-precision simulation tests. Through numerical simulation and model tests, Wichers [15] proved that mooring-assisted dynamic positioning system could significantly reduce the force of mooring lines. Joint positioning has apparent advantages over single positioning. However, research on floating platform positioning system based on the Arctic environment is relatively scarce. The influence of ice load on the positioning capability of floating platforms, especially the dynamic positioning capability, needs to be further discussed.

There is not much research on the design optimization of floating platform in ice region, especially the motion of platform combined with mooring and dynamic positioning system. In this paper, the Kulluk platform equipped with a mooring-assisted dynamic positioning system is chosen as the research object. Dynamic response under wave load, level ice condition, and broken ice floes condition are analyzed. The positioning capability

of the system is evaluated by analyzing the mooring lines' tensions and the thrusters' forces under different environmental loads. Theoretical methods for calculating wave and ice loads are given in Section 2. This section also includes load analysis methods for mooring systems and control methods for dynamic positioning systems. Section 3 introduces the calculation model, including the specific parameters of the model and the composite positioning system design. The accuracy of the model is verified by analyzing the hydrodynamic performance as well as comparing the numerical results of ice loads with the field data. The detailed analysis process is drawn in Section 4. Finally, some conclusion is described in Section 5.

2. Theoretical Method

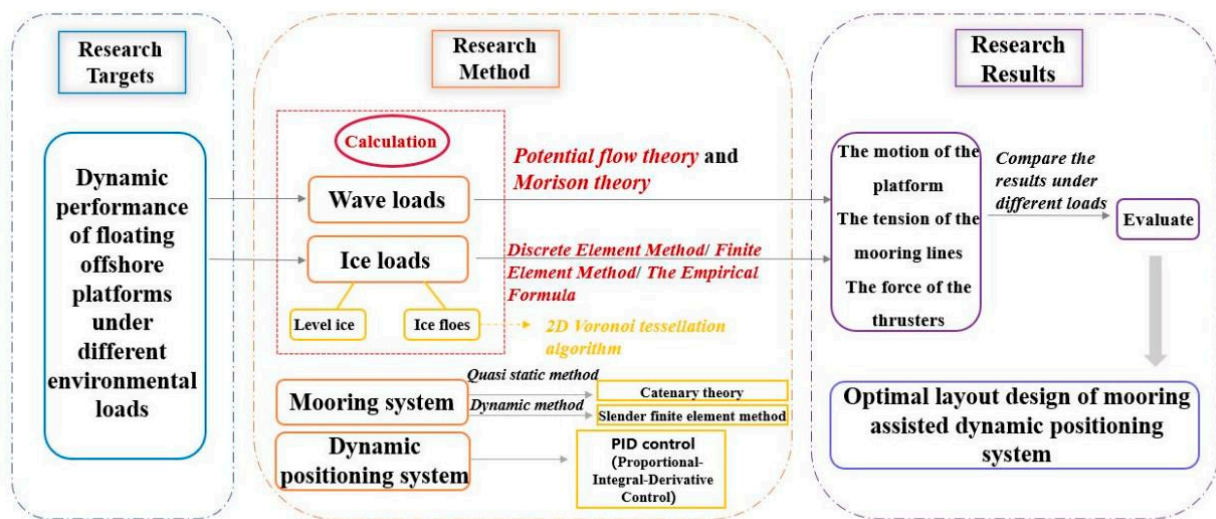The specific calculation process is shown in Figure 1.

Figure 1. Flow chart of calculation and analysis.

2.1. Calculation Method of Wave Load

In this paper, the wave load is calculated using the three-dimensional potential flow theory [16]. It assumes that the fluid is an incompressible ideal fluid and that the motion of the fluid is irrotational. The velocity potential in the flow field $\phi(X, Y, Z, t)$ is expressed as:

$$\phi(X, Y, Z, t) = \phi_0(X, Y, Z, t) + \phi_R(X, Y, Z, t) + \phi_D(X, Y, Z, t) \tag{1}$$

$\phi_0(X, Y, Z, t)$—Velocity potential of the incident wave
$\phi_R(X, Y, Z, t)$—Radiation velocity potential
$\phi_D(X, Y, Z, t)$—Diffraction velocity potential
t—Time
(X, Y, Z)—Coordinate of any point in the flow field

By solving the governing equations of potential flow motion, the velocity potential of the incident wave is:

$$\phi_0(X, Y, Z, t) = \frac{iAg}{\omega} \cdot \frac{\cosh k(z + h)}{\cosh kH} e^{-ik(x \cos \beta + y \sin \beta)} \tag{2}$$

A—Wave amplitude
k—Wave number
β—Wave direction angle
z—Coordinate of water quality point
H—Water depth
ω—Wave frequency

g—Gravitational acceleration

In ideal fluid, the diffraction potential $\phi_D(X, Y, Z, t)$ satisfies the Laplace equation and is expressed as:

$$\nabla^2 \phi_D(X, Y, Z, t) = \frac{\partial^2 \phi_D}{\partial X^2} + \frac{\partial^2 \phi_D}{\partial Y^2} + \frac{\partial^2 \phi_D}{\partial Z^2} = 0 \tag{3}$$

After the diffraction velocity potential of the floating structure is obtained, the Bernoulli equation is used to solve the linear hydrodynamic force acting on the wet surface, which can be expressed as:

$$\vec{p}(X, Y, Z, t) = -\rho \frac{\partial \phi_D(X, Y, Z, t)}{\partial t} - \rho g Z \tag{4}$$

where ρ—Fluid density.

The hydrodynamic force of the floating structure is composed of the Froude-Kralov pressure generated by the incident potential, and the diffraction force generated by the diffraction velocity potential. By integrating the velocity potential of the incident wave, the Froude-Krarov pressure is obtained:

$$\vec{f}_w^I = i\rho\omega \iint\limits_{s} \phi_I \vec{n}_i \mathrm{d}s \tag{5}$$

Diffraction force

$$\vec{f}_w^D = i\rho\omega \iint\limits_{s} \phi_D \vec{n}_i \mathrm{d}s \tag{6}$$

Equations (5) and (6) constitute the first-order wave excitation force, and can be expressed as:

$$\vec{f}_w = \vec{f}_w^I + \vec{f}_w^D \tag{7}$$

Floating structures moving in waves not only make a simple harmonic motion under the first-order wave excitation force, but also suffer from the mean wave drift force that makes them drift. The far field method [17] and the pressure integral method [18] can be used to calculate the mean wave drift force. The far-field method is adopted to the calculation by integrating on the control surface at infinity using the momentum conservation principle. Then the components of the three average second-order forces in the horizontal direction of the floating structure are obtained. The pressure integral method is used to analyze by integrating the surface pressure of structures. The nonlinear pressure on the surface is determined by integrating along the surface of the floating structure. The calculation accurates to the second order, which represents the mean wave drift force.

2.2. Calculation Method of Ice Load

2.2.1. Finite Element Method Based on Fluid-Structure Interaction

LS-Dyna software [19] is used for nonlinear finite element calculation. ALE (Arbitrary Lagrange-Euler) algorithm can be used to analyze the case of ice-water coupling. ALE algorithm can overcome the severe element distortion of numerical computation and realize the dynamic analysis of fluid-structure interaction. ALE algorithm can keep the object boundary condition after deformation, and re-divide the internal element grid so that the topological relation of the grid remains unchanged. The element variables, such as density, energy, and stress tensor, and node velocity vectors in the deformed grid can be transported to the new grid after the re-division. In the ALE algorithm, two layers of the grid overlap together, and the spatial grid can move arbitrarily. The information transmission takes place in these two layers of the grid. The grid can translate, rotate and expand to meet the deformation requirements of the object.

2.2.2. Discrete Element Method

The ice model is constructed by spherical particle elements in the discrete element method [20]. A parallel bonding disk is set up between particle units, and the fracture criterion [21] is used to simulate the ice fragmentation process.

The maximum normal stress and maximum shear stress acting on the bonding disk [22] can be obtained as:

$$\sigma_{\max} = \frac{-\vec{F}_i^n}{A} + \frac{\left|\vec{M}_i^S\right|}{I} R \tag{8}$$

$$\tau_{\max} = \frac{\vec{F}_i^s}{A} + \frac{\left|\vec{M}_i^n\right|}{J} R \tag{9}$$

$\vec{F}_i^n$—Normal force between particles

$\vec{M}_i^n$—Normal moment between particles

$\vec{F}_i^s$—Tangential force between particles

$\vec{M}_i^s$—Tangential moment between particles

R—Radius of the bonding disk

A—Cross-sectional area of the bonding disk

I—Moment of inertia of the bonding disk

J—Polar moment of inertia of the bonding disk

The specific calculation can be expressed as: $A = \pi R^2, J = \frac{1}{2}\pi R^4, I = \frac{1}{4}\pi R^4$ The fracture criterion [20] means that when the maximum stress on the parallel bonding disk exceeds its bonded failure strength, the bonded relationship between the elements will be destroyed.

The tensile failure strength σ^t and shear failure strength τ^s of the bonding units can be expressed as:

$$\sigma^t = \sigma_b^n \tag{10}$$

$$\tau^s = \sigma_b^s + \mu_b \sigma_{\max} \tag{11}$$

σ_b^n—Normal bonding strength
σ_b^s—Tangential bonding strength

$$\sigma_b^n = \sigma_b^s$$

where μ_b—Coefficient of internal friction.

$$\mu_b = \tan \varphi$$

where φ—Angle of internal friction.

The simulation of broken ice area with different ice thickness, ice concentration, and ice floes size is completed based on the two-dimensional Voronoi tessellation algorithm [23].

2.3. Method for Load Analysis of Mooring Systems

The load calculation methods of the mooring system include the quasi-static method and dynamic method. The quasi-static method is based on catenary theory [24], which assumes the mooring line as a two-dimensional model and only considers its gravity, ignoring the dynamic action of the fluid. For the multi-moored positioning system, when the floating foundation drift distance is y, it can be expressed as:

$$l_i - l_0 + x_0 + y\cos(\pi - \alpha_i) = x_i \tag{12}$$

where, subscript 0 represents the position when the initial position is balanced; subscript i indicates the position of the i-th mooring line after drift motion; a_i represents the angle between the mooring lines plane and the drift direction. After drifting y, α'_i can be expressed as: $\alpha'_i = ai + \gamma_i$, $\gamma_i = arcsin(\frac{y}{x_i}sina_i)$. Therefore, the horizontal tension of the corresponding mooring line can be found. Then, for the positioning system with N mooring lines, the horizontal mooring force of the floating foundation, also called system recovery force, is:

$$F = \sum_{i=1}^{N} R_i \cos \alpha'_i \tag{13}$$

The dynamic calculation method uses a finite element method based on slender body theory [25]. In the slender body theory, the mooring line is regarded as a continuous elastic medium. The static equilibrium and dynamic response of the mooring system are solved by the finite element method. The stress state at any point on a slender body is represented by the total internal force F and the total moment M acting on the central line. According to the balance of force and moment in the unit arc length segment, the motion equation of the mooring line can be expressed as follows:

$$F' + q = \rho \ddot{r} \tag{14}$$

$$M' + r' \times F + m = 0 \tag{15}$$

q—External force per unit length
ρ—Mass per unit length
m—Moment applied per unit length

2.4. The Control Method of the Dynamic Positioning System

The control system will calculate the force required for positioning according to the environmental information and position motion information, and distribute the force instructions to each thruster reasonably. PID control (proportional-integral-derivative control) [26] is adopted in this paper. The three-degree-of-freedom PID control method in the horizontal plane of the dynamic positioning system is expressed as:

$$\tau_{con} = -K_p \Delta x - K_d \dot{x} - K_i \int_0^t \Delta x(\tau) \mathrm{d}\tau \tag{16}$$

where, x is the three-degree-of-freedom position of the horizontal plane of the structure; Δx is the deviation between the control point of the structure and the position of the target; K_p, K_i and K_d are proportional gain coefficient, integral gain coefficient, and derivative gain coefficient, respectively.

After calculating the angle of each thruster and the force generated, the power consumed by each thruster can be expressed as:

$$P = \frac{2\pi K_Q}{K_T^{3/2} \rho^{1/2} D} T^{\frac{3}{2}} \tag{17}$$

where, T and Q are the thrust and torque of thrusters, respectively; n is thruster speed; D is thruster diameter; K_T and K_Q are the thrust coefficient and torque coefficient of thruster, respectively.

3. Numerical Model and Validation

3.1. Model Information and Operating Condition Introduction

Due to the availability of long-term ice load field data, the numerical calculation model of Kulluk platform is constructed in this paper, as shown in Figure 2a. The specific full-scale design parameters of the platform, including top diameter, waterline diameter, bottom diameter, cone angle, depth, and draft, are shown in Figure 2b. The designs of the

mooring-assisted dynamic positioning system are presented in Figure 3, with 16 different schemes. There are four cases according to the number of mooring lines: 4, 8, 12, and 16. The layout of the dynamic positioning system also has four different cases due to the number and position of azimuthing thrusters. The water depth calculated in this paper is 150 m. The total length of a single mooring line is 773.72 m. Under wave load, the upper limit of force provided by a single thruster is set to 5000 N. Under level ice condition, it is 100,000 N. The ice floes condition is 12,000 N. According to the environmental conditions of Beaufort Sea provided in ISO 19906 (2019) [27], the operating conditions in this paper are selected as shown in Table 1. In this paper, the SESAM software [28] developed by DNV-GL is used for calculation and analysis. The data analysis graphs are drawn by Origin software.

(a)　　　　　　　　　　　　　　　　　　**(b)**
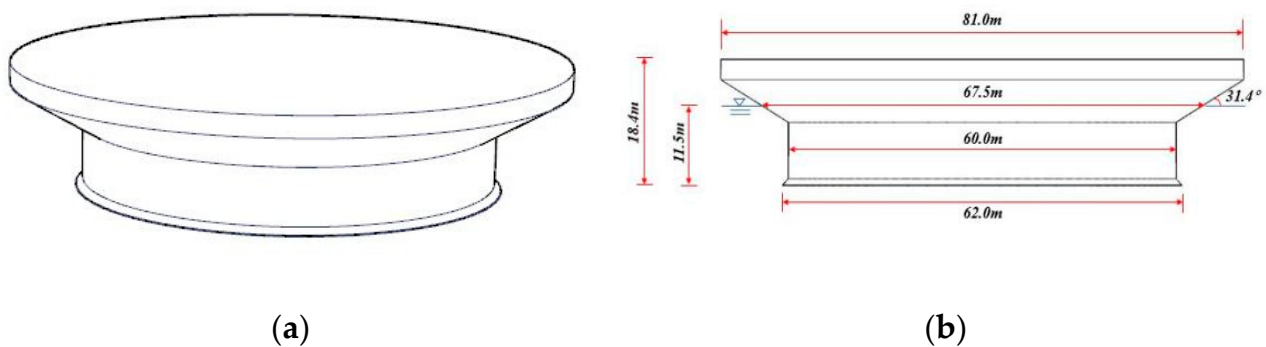
Figure 2. Schematic of the Kulluk platform. (**a**) Numerical model; (**b**) Platform design parameter information.

Table 1. The environmental conditions in this paper.

Parameters	Values
Significant wave height (m)	3.7
Spectral peak period (s)	6.7
Thickness of the level ice (m)	1.8
Ice speed (m/s)	0.1
Thickness of the broken ice floes (m)	1.8
Average size of the ice floes (m^2)	50
Concentration of the broken ice floes area (%)	80
Current speed (m/s)	0.4

3.2. Hydrodynamic Performance Prediction and Mesh Convergence Verification

The platform's motion response, including heave, pitch, and roll motion, is predicted by the frequency domain analysis method. It can indicate the motion in these three directions with high precision. Based on the data obtained from frequency domain analysis, the mesh convergence of the computing model of the platform is analyzed. In this paper, three different sizes of mesh elements (0.75 m × 0.75 m, 1.00 m × 1.00 m, and 1.25 m × 1.25 m) are used to construct full-scale numerical models. The differences in the mesh models are demonstrated in Figure 4. The hydrodynamic parameters include RAO (Response Amplitude Operator), first-order wave force, and second-order wave force. The second-order wave force is calculated by the far-field method and pressure integral method. As can be seen from Figure 5, the calculation results of the three groups of different mesh models are close. The influence of mesh numbers on numerical simulation can be excluded. Finally, Model 1, with the largest number of meshes, is selected for the subsequent time domain calculation.
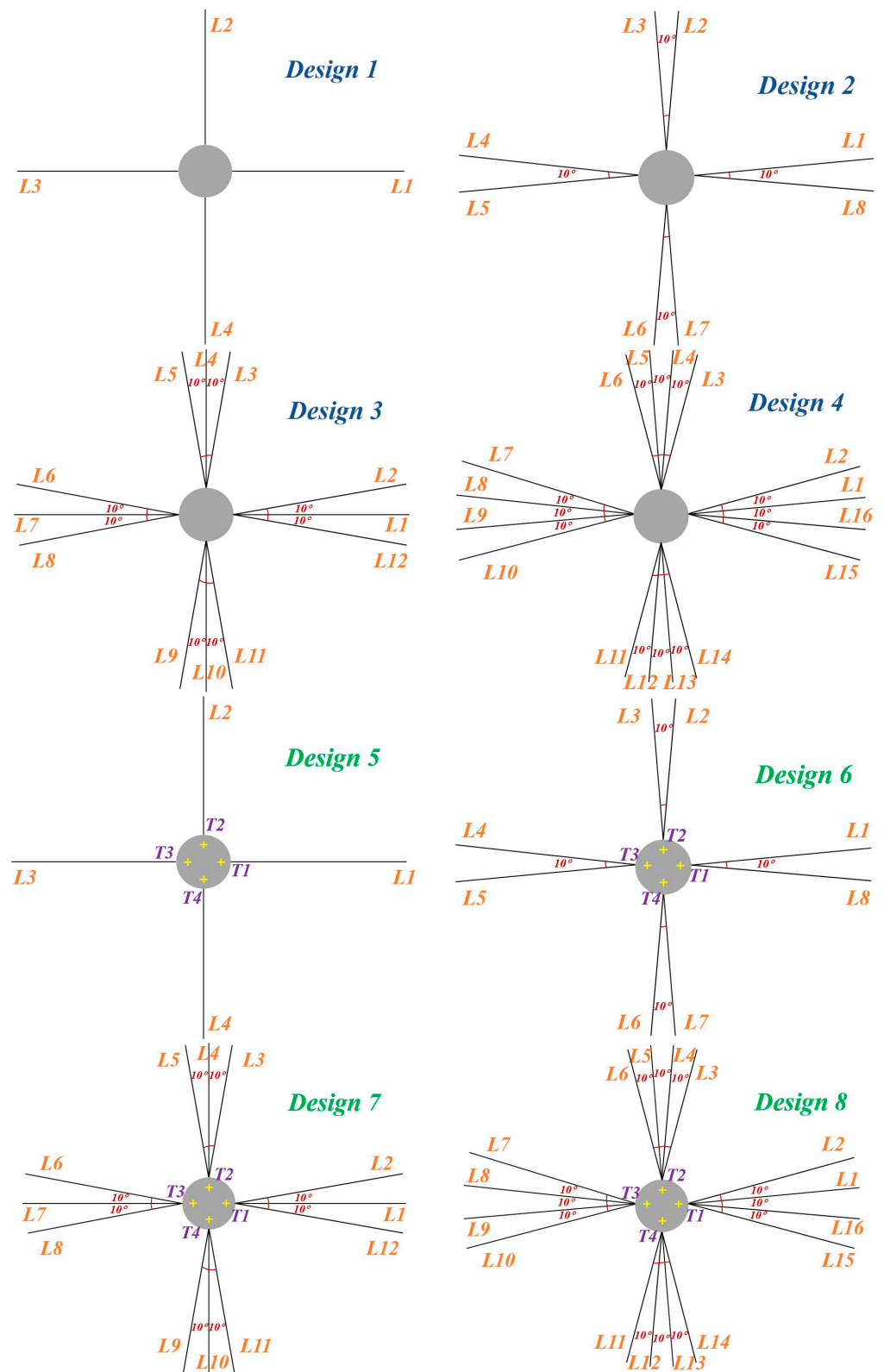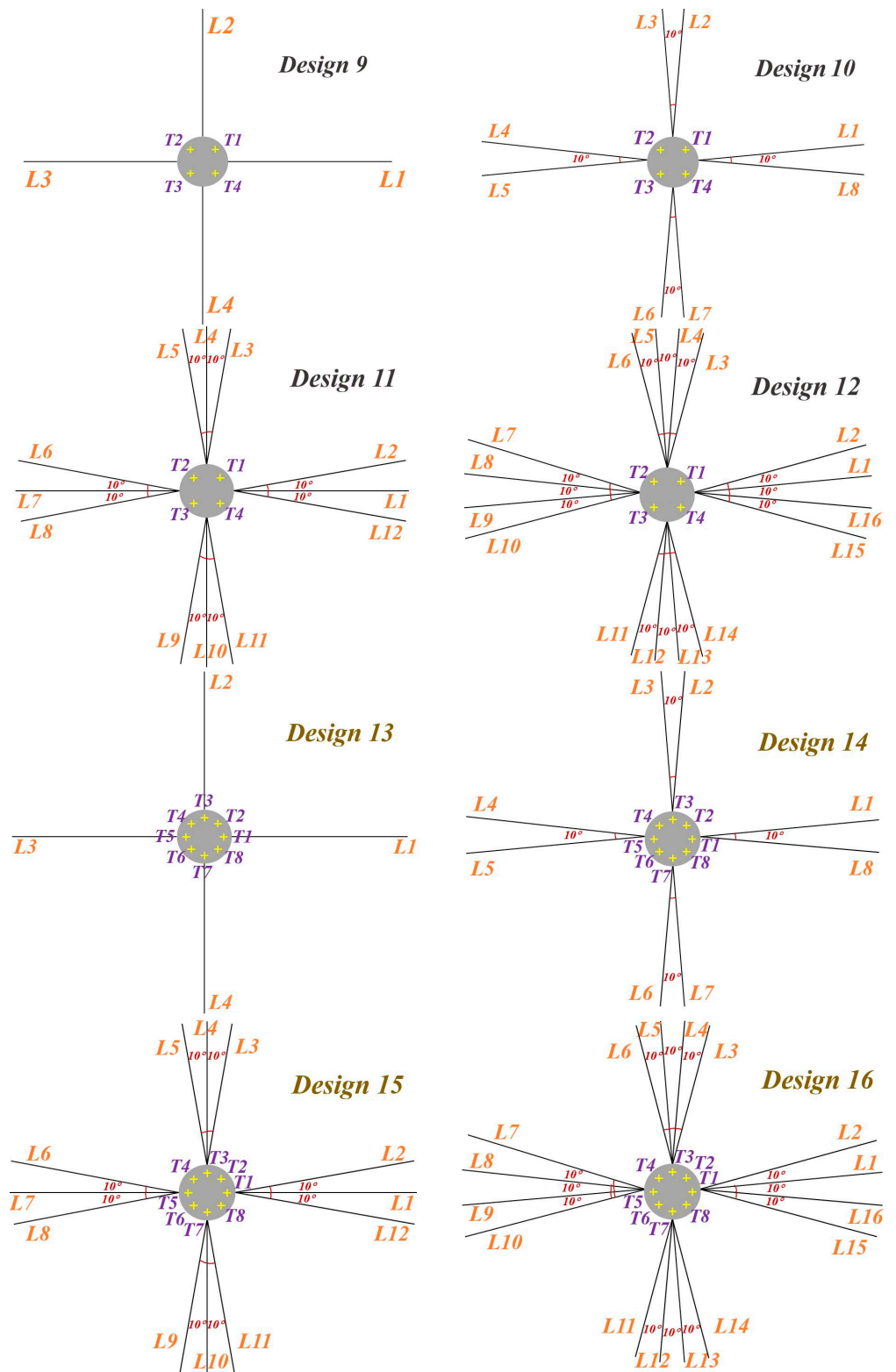
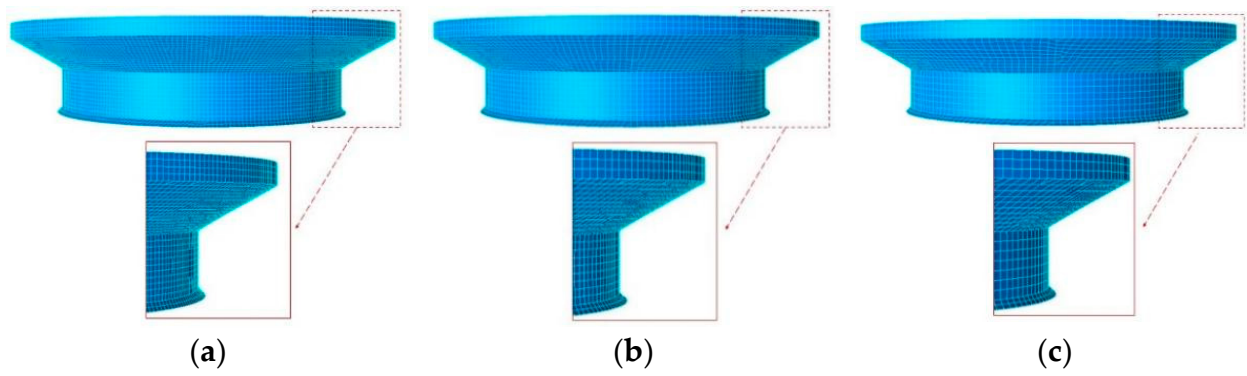**Figure 3.** *Cont.*

Figure 3. Design of positioning system.

Figure 4. Mesh model. (**a**) Model 1 (0.75 m × 0.75 m); (**b**) Model 2 (1.00 m × 1.00 m); (**c**) Model 3 (1.25 m × 1.25 m).

Figure 5. *Cont.*

(e)

(f)
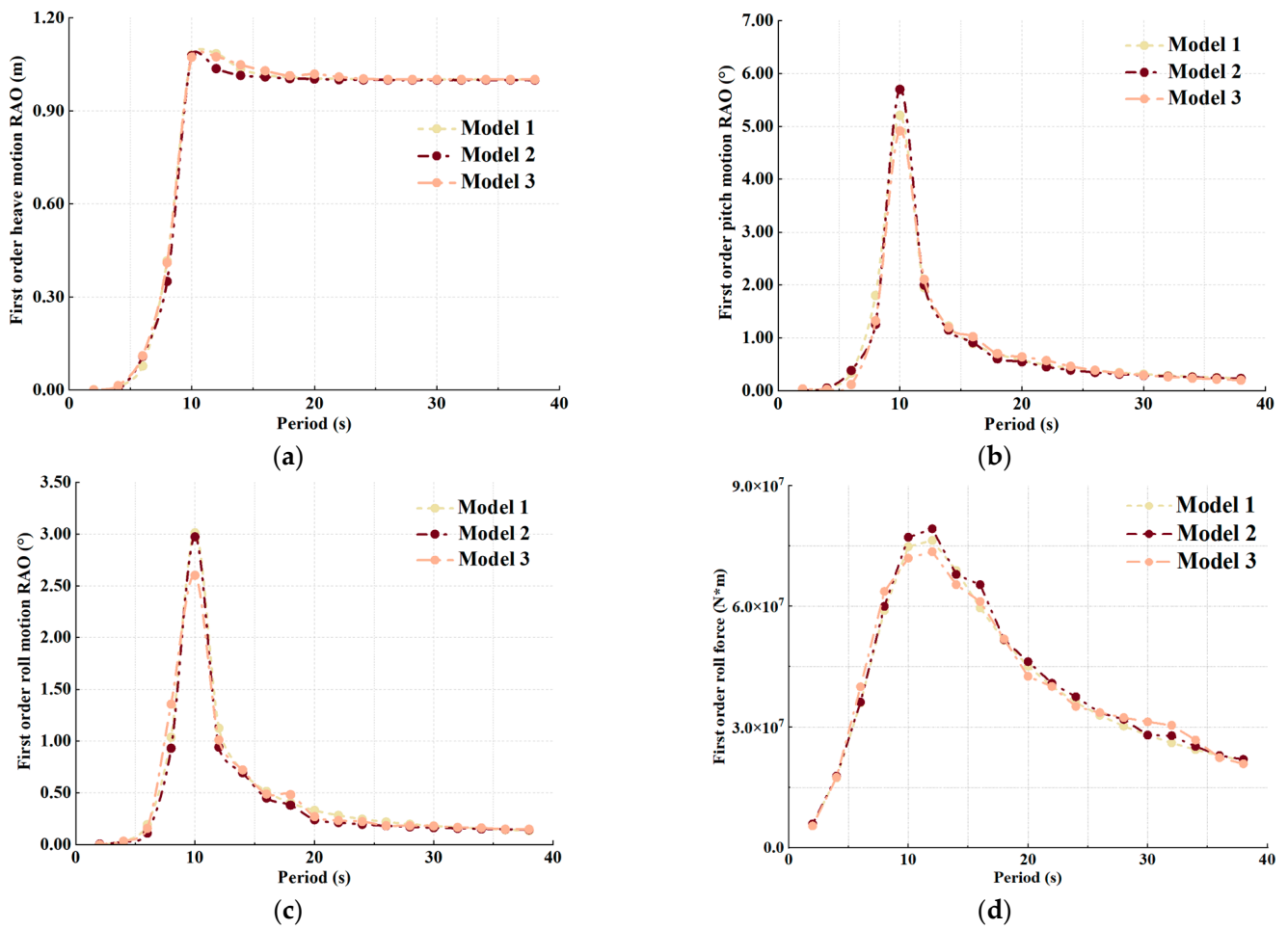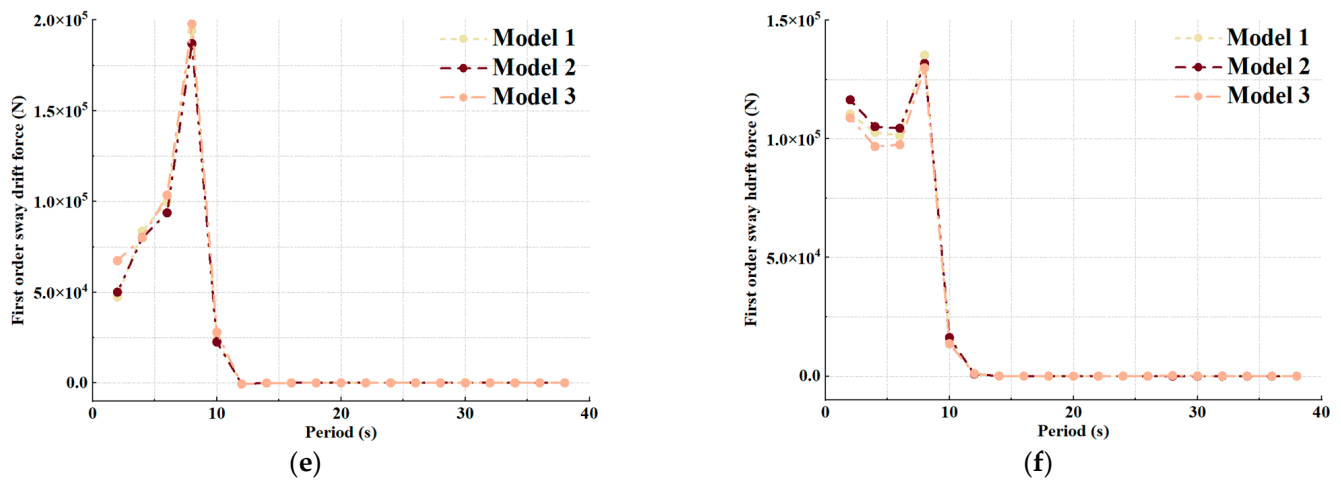
Figure 5. Mesh convergence verification. (**a**) First-order heave motion; (**b**) First-order pitch motion; (**c**) First-order roll motion; (**d**) First-order roll moment; (**e**) Mean drift force in the sway by the far-field method; (**f**) Mean drift force in the sway by direct pressure integral method.

3.3. Comparison of Ice Load Simulation Methods

In this paper, finite element method based the fluid-structure interaction and discrete element method are used to analyze the interaction between ice and the Kulluk platform. These two methods use the same calculation time and working conditions, and the schematic diagram of numerical simulation is observed in Figure 6. Figure 7 compares the ice load values of the Kulluk platform under the different methods. The time history curves all show an irregular trend, and the peak value of the ice load appears almost simultaneously [29]. Using the finite element method, the peak value is larger and the fluctuation is more violent. That is because the fluid does not have the buffer effect by this way. More force between the ice and the structure will be generated. The setting of erosion contacts and the invalidation of grid elements also make the contact frequency between ice and structures lower. Considering the time and calculation accuracy, we choose the discrete element method to calculate the subsequent ice load. At present, it is very difficult to conduct scale-model tests on the interaction between floating offshore platforms and sea ice. Therefore, the accuracy of numerical calculation is verified by comparing with field data. The Kulluk platform was used for offshore operations in the Beaufort area and had complete ice load field data. Figure 8 compares the numerical simulation results with the field data in terms of ice thickness and ice concentration. The results satisfy the upper limit of ice load defined in the Kulluk research report [6], which can be used for further analysis.

(a)

(b)
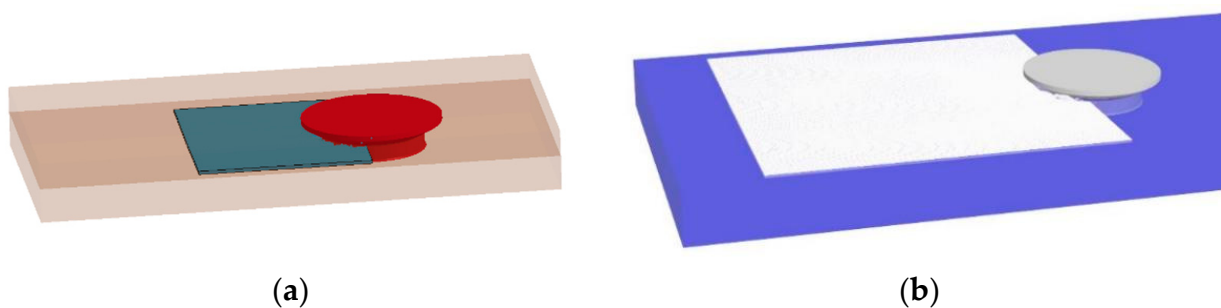
Figure 6. Numerical calculation of interaction between ice and structures. (**a**) Finite element method; (**b**) Discrete element method.
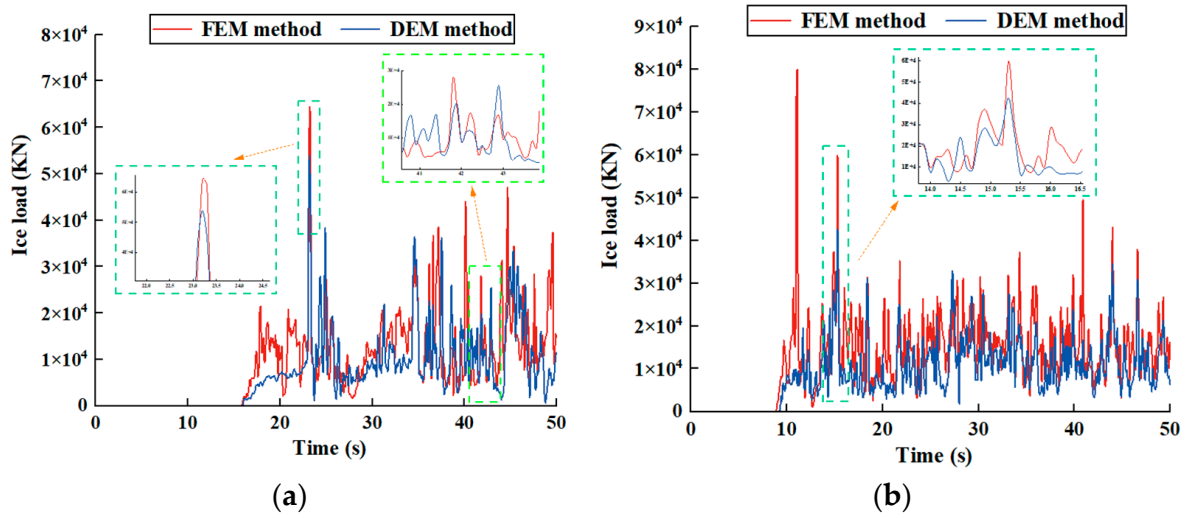
Figure 7. Comparison of different ice load calculation methods. (**a**) 0.6 m/s ice speed; (**b**) 1.2 m/s ice speed.
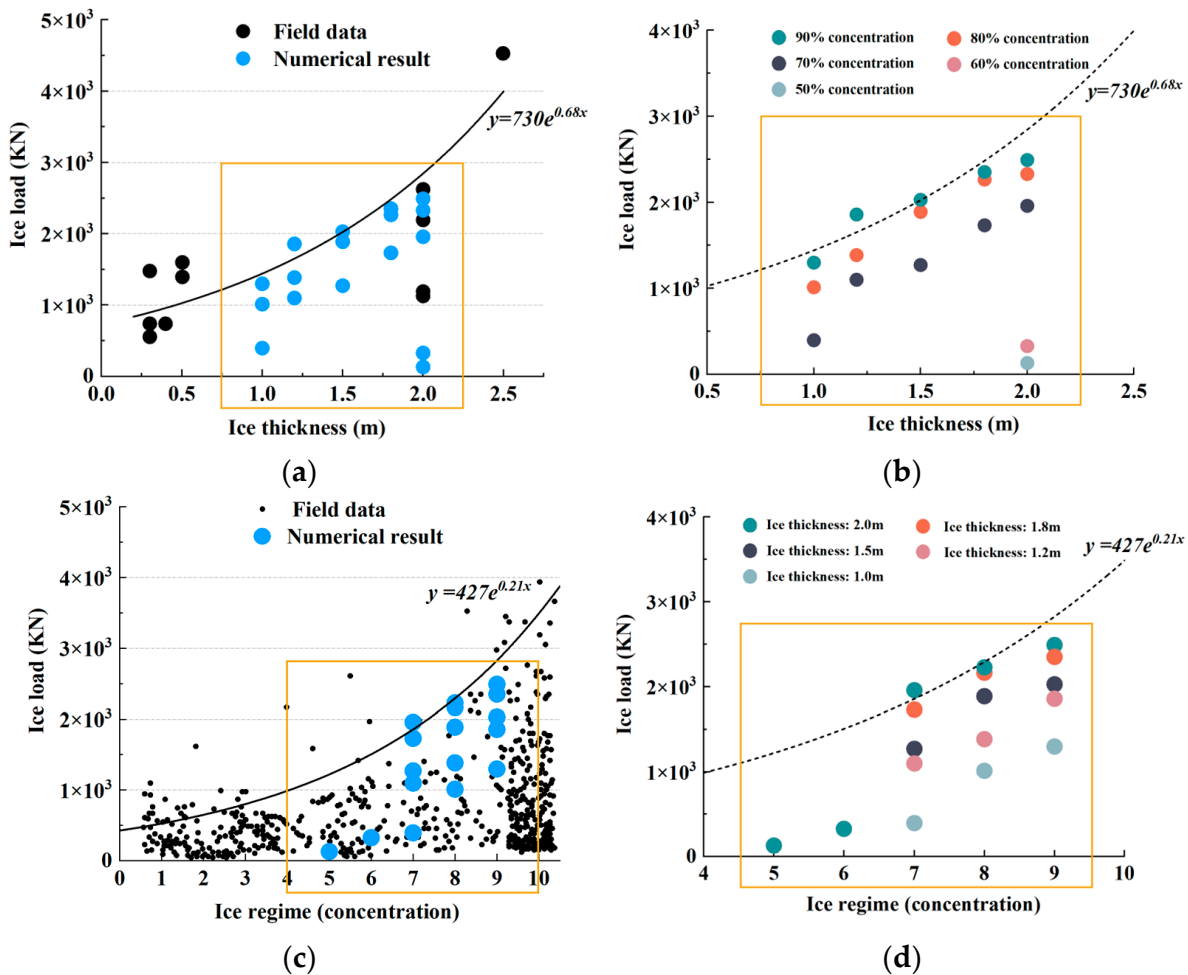

Figure 8. Comparison between the numerical simulation results and field data. (**a**) Ice thickness; (**b**) Ice thickness (Different colors represent different ice concentrations); (**c**) Ice concentration; (**d**) Ice concentration (Different colors represent different ice thicknesses).

4. Analysis of the Results

4.1. Mooring Lines Tension under Different Positioning Modes

Figure 9 depicts the average tension of the mooring lines under different environmental loads and positioning modes. Different colors represent different dynamic positioning systems. This set of pictures can comprehensively compare the tensions under various design schemes. It includes the influence of the different number of mooring lines on the tension of the mooring system under the same dynamic positioning system, as well as the tension situation under the same number of mooring lines and different arrangements of thrusters. It can be seen that the mooring-assisted dynamic positioning system can effectively reduce the tension of the mooring lines and improve its service life compared to the positioning system with only the mooring system. The number of mooring lines has a significant influence on the average tension of the mooring system, especially when the positioning system has no thruster. When the mooring system is arranged in the same way, there is no significant difference in the tension between the schemes equipped with thrusters.
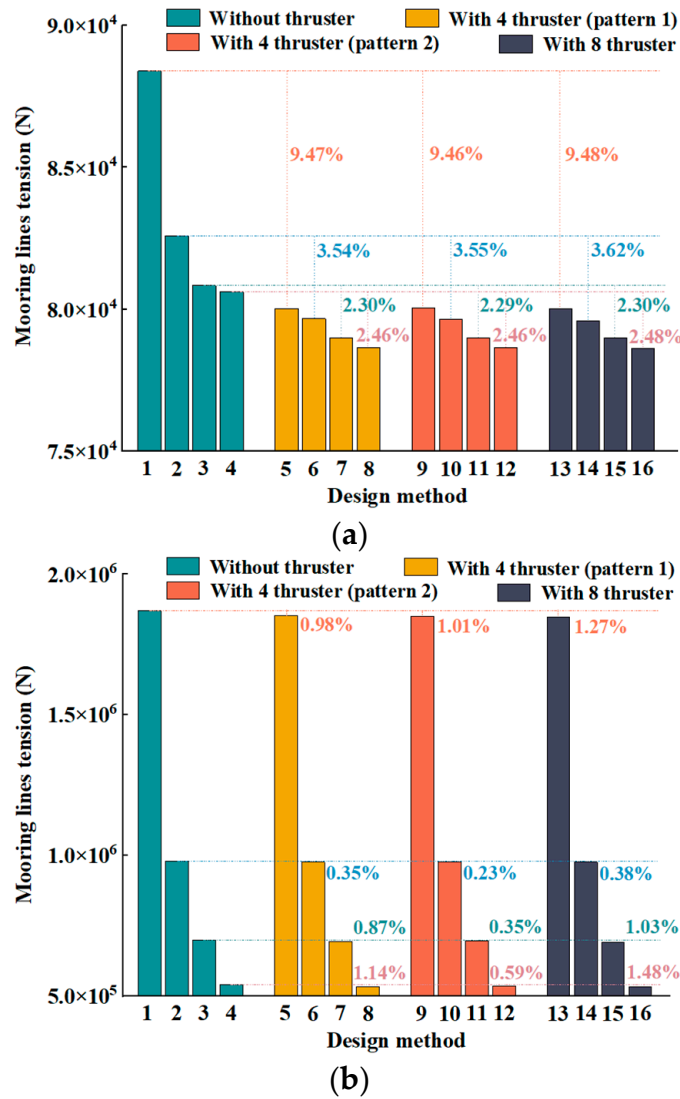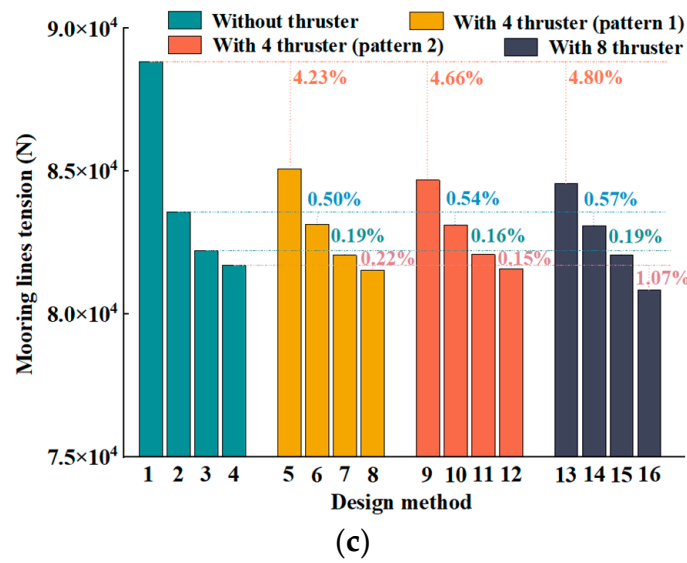
(a)

(b)

Figure 9. *Cont.*

Figure 9. Tension of the mooring lines under different environmental loads and positioning modes. (**a**) Wave condition; (**b**) Level ice condition; (**c**) Ice floes condition.

Under level ice condition, the tension of the mooring line is much greater than that under wave condition and broken ice floes condition. The difference between mooring line tension under composite and single positioning system is less than 1.5%. This is because the level ice will cause the platform to have a significant deviation, and the mooring system will provide a great force to keep the platform in a relatively stable state [10]. At this stage, the mooring line remains tensioned and the thrusters play little role. If the thrusters provide too much force at this time, the platform will have a considerable yaw motion, resulting in the winding between the mooring lines. Meanwhile, the platform collides with level ice. The broken ice could come into contact with the thrusters, which could deform and damage the blades, rendering them ineffective [30–32]. In contrast, under wave load, the design of different positioning modes has a more obvious correlation with the tension of the mooring lines. Both the mooring system and dynamic positioning system can play an important role. Under the level ice condition, the mooring system is mainly used for positioning. The dynamic positioning system plays an auxiliary role but has little effect. Compared with level ice condition, the dynamic positioning system plays a significant role under the broken ice floes condition. However, there is no significant difference in the tension of mooring lines under different numbers and arrangements of thrusters.
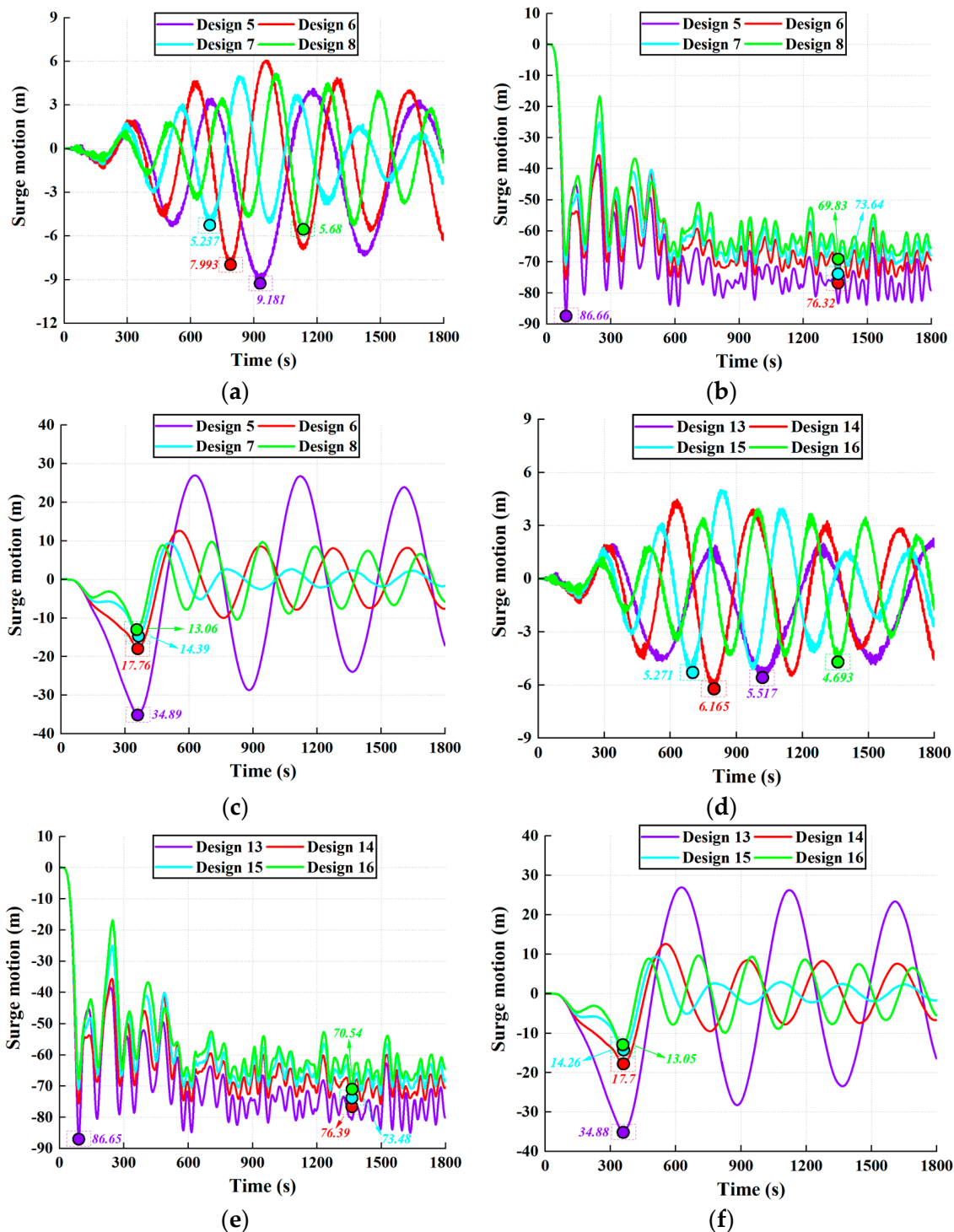
4.2. Platform Motion under Different Positioning Modes

This paper analyzes the platform's motion under different environmental conditions and positioning modes. The positioning capability of the mooring-assisted dynamic positioning system is evaluated from two aspects.

4.2.1. Surge, Sway and Yaw Motion of the Platform under Different Environmental Loads

This section investigates the effect of the other positioning mode's change on the platform motion when one of the mooring system and dynamic positioning system is the same. Two design schemes of four thrusters (Pattern 1) and eight thrusters are taken as examples to carry out the research. Figure 10 describe the platform's surge motion under different environmental loads. Under wave load, the positioning effect of the eight-thrusters design is better than that of the four-thrusters design. With the same number of mooring lines, the surge motions decrease by 39.9%, 22.9%, 0.3%, and 17.4%, respectively. However, under level ice and broken ice floes, the surge motion of the platform equipped with the same number of mooring lines and different thruster forms is less than 1%. This is

similar to the conclusion in Section 4.1, indicating that the positioning effect of the dynamic positioning system under the ice load is not as obvious as that of the mooring system.

Figure 10. Surge motion of the platform under different environmental loads. (**a**) Surge motion in four-thrusters (Pattern 1) design under wave load; (**b**) Surge motion in four-thrusters (Pattern 1) design under level ice; (**c**) Surge motion in four-thrusters (Pattern 1) design under broken ice floes; (**d**) Surge motion in eight-thrusters design under wave load; (**e**) Surge motion in eight-thrusters design under level ice; (**f**) Surge motion in eight-thrusters design under broken ice floes.

It can be seen from the figures that the number of mooring lines has a significant impact on the platform's surge motion. The greater the number of mooring lines, the smaller

the surge motion of the platform. The positioning capability of the platform is stronger. This conclusion can be verified under different environmental loads, especially under the condition of broken ice floes. Compared with a single mooring line, the positioning effect of multiple mooring lines in the same direction can be improved by more than 50%. Therefore, the mooring-assisted dynamic positioning system of the offshore platform applied in the Arctic region should provide a sufficient number of mooring lines. The four main directions (the symmetry axis direction of the symmetrical structure) of the double-symmetric structure should be equipped with multiple mooring lines acting simultaneously to ensure the safe operation of the platform.

The sway and yaw motion of the platform with a dynamic positioning system is not only affected by the external loads but also aggravated by the force of the thrusters. Figure 11 reveal the platform's maximum sway and yaw motion under different environmental loads. As described in the figures, the sway motion of the platform under the wave load is much smaller than that under the broken ice floes condition. The sway motion under level ice condition is the most violent and is greatly affected by the number of thrusters. Without considering the influence of the mooring system, the increase in the number of thrusters will lead to a more significant maximum sway motion of the platform under the ice load. The upper force limit for each thruster in this paper is the same, and the design of eight thrusters will provide additional force in all directions other than the main direction. This is different from the effect of the force in the main direction supplied by the mooring system and the four-thrusters (Pattern 1) design. It will slightly reduce the platform's surge motion and lead to the corresponding increase of the platform's sway motion and yaw motion. The motion of the platform under the condition that the mooring system and dynamic positioning system are changed simultaneously will be studied in the following section.
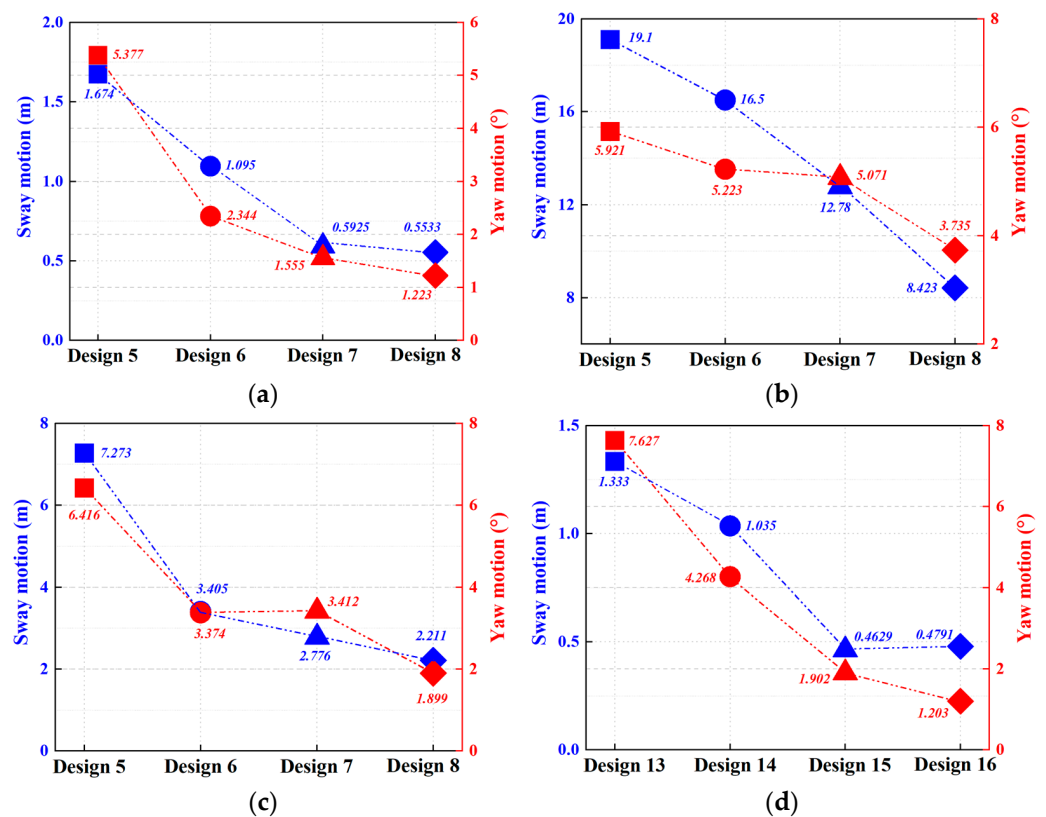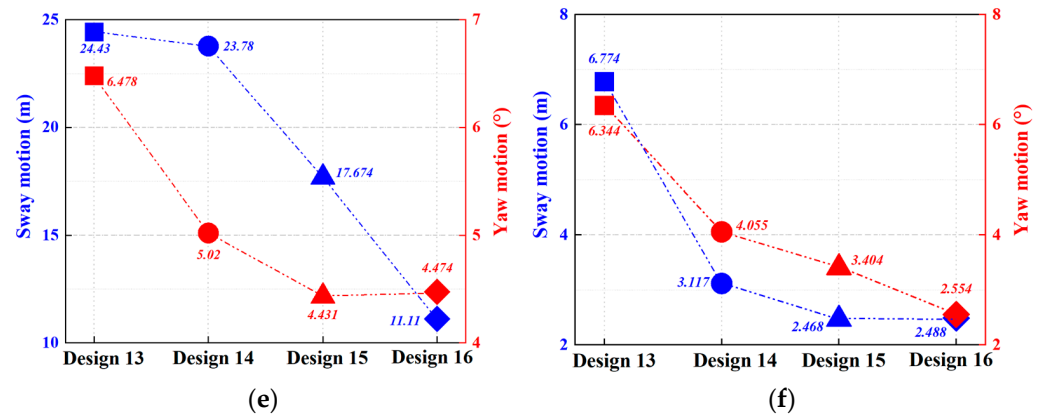

Figure 11. *Cont.*

Figure 11. Sway and yaw motion of the platform under different environmental loads. (**a**) Sway and yaw motion in four-thrusters (Pattern 1) design under wave load; (**b**) Sway and yaw motion in four-thrusters (Pattern 1) design under level ice; (**c**) Sway and yaw motion in four-thrusters (Pattern 1) design under broken ice floes; (**d**) Sway and yaw motion in eight-thrusters design under wave load; (**e**) Sway and yaw motion in eight-thrusters design under level ice; (**f**) Sway and yaw motion in eight-thrusters design under broken ice floes.

Under different mooring systems, the maximum yaw motion varies greatly. The difference is particularly significant under wave load. In the case of the four-thrusters (Pattern 1) design, compared with the motion under a single mooring line in the same direction, the yaw motion of the platform under the other three mooring systems with multiple mooring lines in the same direction decreased by 56.4%, 71.1%, and 77.3% respectively. For the eight-thrusters design, these values are 44.04%, 75.06%, and 84.23%, respectively. However, the different number of thrusters has little influence on the yaw motion of the platform with a fixed mooring system, which is the same under the three environmental loads.

Therefore, in addition to energy efficiency, the positioning effect is an essential factor in the design of thrusters. An appropriate number of thrusters can reduce the force of the mooring system and the overall deviation of the platform to a certain extent. Exceeding certain limits, such as arranging too many thrusters or providing too much force, can result in complex and difficult to control platform motion.

4.2.2. Motion Trajectories of the Platform under Different Positioning Modes

Figure 12 show the motion trajectories of the platform under different positioning modes in different environments. In this section, the positioning capabilities of different mooring systems and dynamic positioning systems can be compared under any combination. As can be seen from the trajectories in the figures, the platform's surge motion under the mooring-assisted dynamic positioning system is smaller than that under the mooring positioning system. The dynamic positioning system has a significant influence on sway motion and roll motion, and the different number and arrangement of thrusters will result in different positioning effects.

The eight-thrusters design works best under wave load. Compared with other dynamic positioning schemes, the platform's surge motion, sway motion, and yaw motion are all reduced. With the same number of thrusters but different positions, the positioning capability of the design is not significantly different. But the route of the platform motion is affected by the thrust direction to produce a particular deviation. When the force provided by the thrusters and the tension provided by the mooring system are not in the same direction (as in Designs 9 and 13), the sway motion of the platform is correspondingly reduced, especially if the number of mooring lines is small.

The surge motion of the platform is particularly intense under the condition of level ice. Unlike other environmental loads, the platform does not have frequent reciprocating motion. The positioning system does not work until the platform reaches a particular position. Dynamic positioning system plays a more prominent role in multi-mooring

lines arrangement. Figure 12a clearly reflects the inapplicability of the multi-thrusters less-mooring-lines system in positioning. By comparing Figure 12d,g,j, it can be seen that the coordination of 8 thrusters and 12 mooring lines can achieve the optimal positioning effect. This is the reason of the configuration of three mooring lines in one direction. The middle lines (L1, L7) and thrusters (T1, T5) work together to provide a large recovery force in the main direction. In the other directions, the thrusters (T2, T4, T6, T8), with the assistance of the mooring lines (L2, L6, L8, L12) on both sides, reduce the force component to avoid significant sway motion. The positioning system with four thrusters (Pattern 1) and 16 mooring lines also has good positioning ability. It can be seen that under severe environmental loads, the main direction of the platform needs to be equipped with thrusters or mooring lines to minimize the impact of external loads.
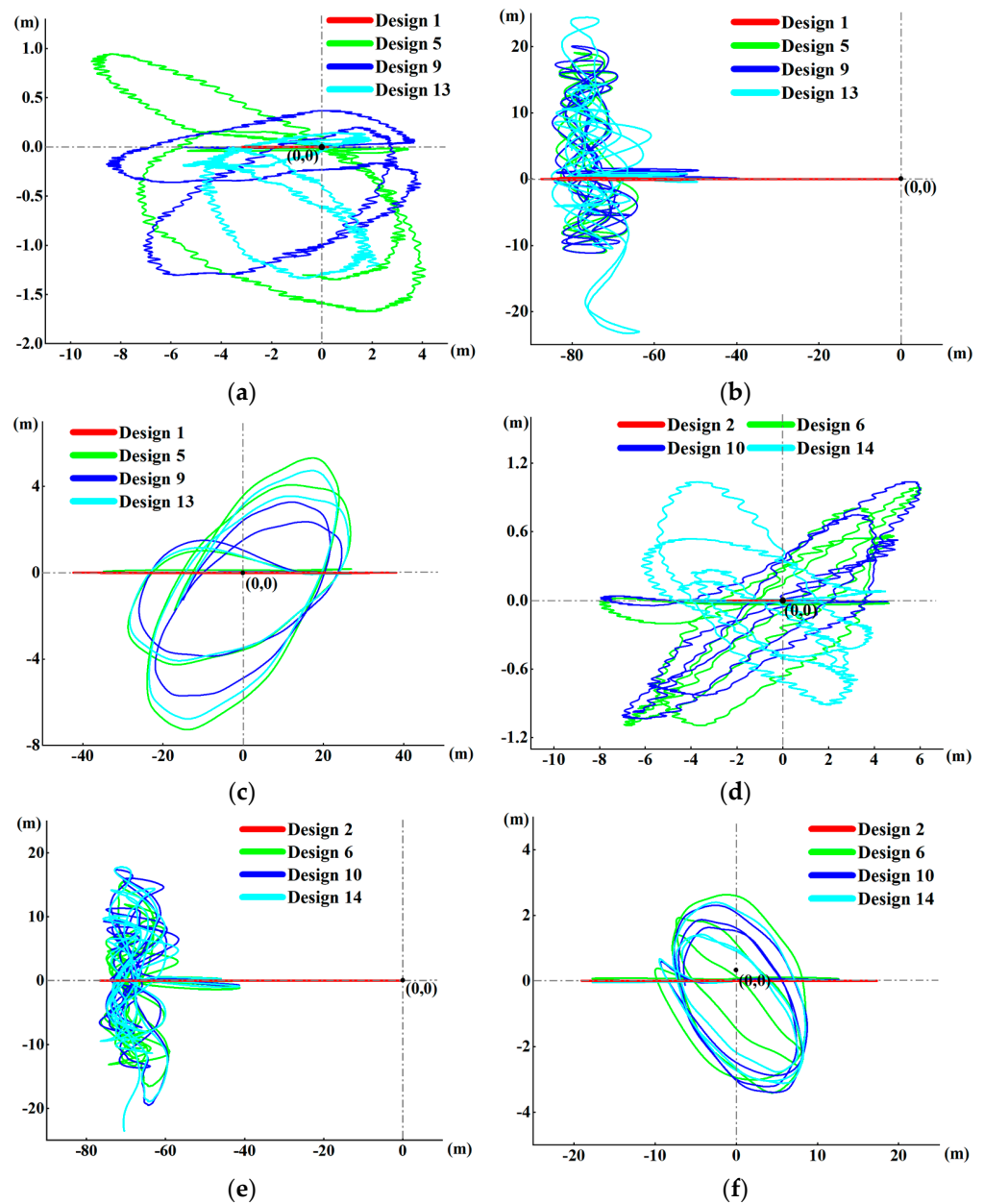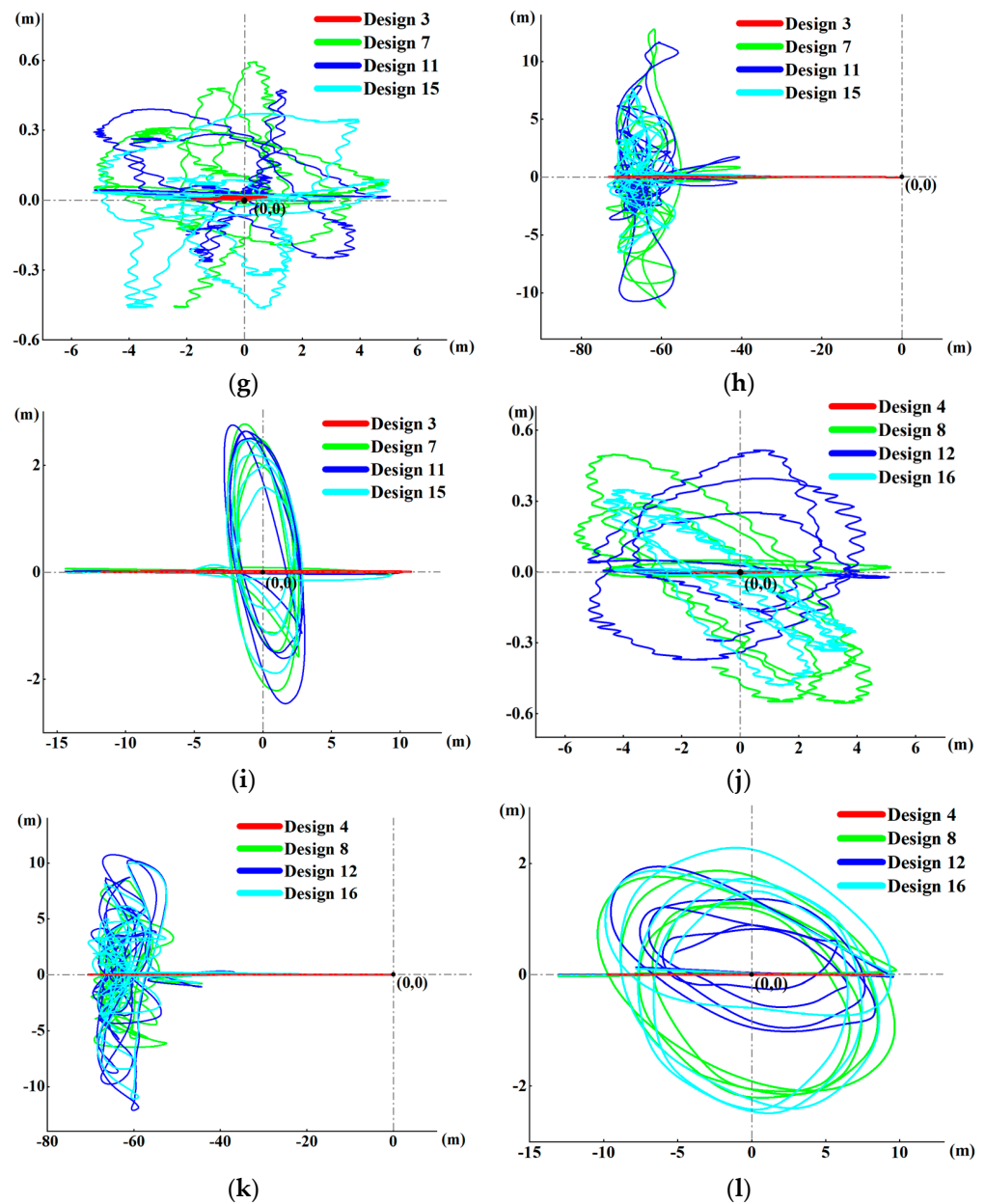

Figure 12. *Cont.*

Figure 12. Motion trajectories of the platform under different positioning modes. (**a**) Motion trajectories diagram of the platform with different dynamic positioning modes and four mooring lines under wave load; (**b**) Motion trajectories diagram of the platform with different dynamic positioning modes and four mooring lines under level ice; (**c**) Motion trajectories diagram of the platform with different dynamic positioning modes and four mooring lines under broken ice floes; (**d**) Motion trajectories diagram of the platform with different dynamic positioning modes and eight mooring lines under wave load; (**e**) Motion trajectories diagram of the platform with different dynamic positioning modes and eight mooring lines under level ice; (**f**) Motion trajectories diagram of the platform with different dynamic positioning modes and eight mooring lines under broken ice floes; (**g**) Motion trajectories diagram of the platform with different dynamic positioning modes and 12 mooring lines under wave load; (**h**) Motion trajectories diagram of the platform with different dynamic positioning modes and 12 mooring lines under level ice; (**i**) Motion trajectories diagram of the platform with different dynamic positioning modes and 12 mooring lines under broken ice floes; (**j**) Motion trajectories diagram of the platform with different dynamic positioning modes and 16 mooring lines under wave

load; (**k**) Motion trajectories diagram of the platform with different dynamic positioning modes and 16 mooring lines under level ice; (**l**) Motion trajectories diagram of the platform with different dynamic positioning modes and 16 mooring lines under broken ice floes.

Under the broken ice floes condition, the motion trajectories of the platform are similar with different numbers and arrangements of thrusters. By comparing Figure 12b,e,h,k, it can be seen that the positioning effect of the 12 mooring lines assisted dynamic positioning system is the best. Similar to the conclusion obtained under level ice condition, the mooring lines arrangement in the main direction is beneficial to reduce the platform deviation, especially the surge motion. Meanwhile, the arrangement of the four-thrusters (Pattern 2) design has the best positioning effect on the platform under the broken ice floes condition. This is consistent with the phenomenon under wave load, where the thrusters (not the main direction) and the mooring lines (the main direction) should provide the decisive recovery force in their respective directions.

In future studies, we will try to use a machine learning-based method [33] to predict the trajectory of the platform in a longer time range.

5. Conclusions

This paper studies the positioning effect of the Kulluk platform equipped with a mooring-assisted dynamic positioning system under the conditions of the wave, level ice, and broken ice floes. The mesh convergence of the numerical model is analyzed. The finite element method based on the fluid-structure interaction and the discrete element method are compared in calculating of the ice load. The numerical results of the ice load are compared with the field data. The results coincide well, which verifies the accuracy of the calculation model. The following conclusions can be drawn by analyzing the maximum surge, sway, and yaw motion of the platform under different positioning modes as well as the motion trajectories in the full time-domain:

1. Compared with the mooring system, the mooring-assisted dynamic positioning system can effectively reduce the tension of the mooring lines, but the effect is not significant enough under the condition of level ice. In the composite positioning system, the mooring system plays a greater role than the dynamic positioning system, which is the main part of providing the recovery force for the platform. Under the same mooring arrangement, the change in the number and position of thrusters will not have a significant impact on the average tension of the mooring system.

2. Compared with a mooring system, a mooring-assisted dynamic positioning system can reduce platform deviation. The influence of a dynamic positioning system on sway and yaw motion under different environmental loads should be considered comprehensively in the design. Mooring lines or thrusters should be arranged in the main direction of the platform structure to avoid excessive surge motion. In the design scheme of this paper, eight thrusters and four thrusters (Pattern 2) have a better positioning effect on the platform. The arrangement of thrusters in the direction of the non-mooring system is more conducive to the stability of the platform.

3. Compared with wave condition, ice condition has a higher correlation with different positioning methods. Ice loads can lead to greater differences in platform motion responses. The tension of the mooring system changes more considerably under level ice. The maximum surge, sway and yaw motion of the platform under different design schemes also fluctuate the most in level ice condition. From the time-domain analysis, it can be observed that the period and amplitude of the platform's reciprocating motion under the broken ice floes are more obvious than that under the wave loads.

In future research, the method presented in this paper can be used for the compound failure of the mooring-assisted dynamic positioning system of the arctic floating platform. This allows for a better assessment of the system's ability to respond to emergencies during offshore operations. On this basis, the scale-model test of floating offshore platform operating in the ice area will be carried out, combined with the numerical simulation and

field data, to provide reference for the design of the platform, and then applied to the actual project.

References

1. Berkman, P.A.; Young, O.R. Governance and Environmental Change in the Arctic Ocean. *Science* **2009**, *324*, 339–340. [CrossRef]
2. Idris, A.J.; Montasir, O.A.; Anurag, Y.; Zafarullah, N.; Akihiko, N. Optimisation of mooring line parameters for offshore floating structures: A review paper. *Ocean. Eng.* **2022**, *247*, 110644.
3. Zhang, H.; Wang, H.; Cai, X.; Xie, J.; Wang, Y.; Zhang, N. Novel method for designing and optimising the floating platforms of offshore wind turbines. *Ocean. Eng.* **2022**, *266 Pt 2*, 112781. [CrossRef]
4. Henderson, J.; Loe, J.S. The Prospects and Challenges for Arctic Oil Development. *Oil Gas Energy Law J.* **2016**, *14*.
5. Amaechi, C.V.; Reda, A.; Butler, H.O.; Ja'e, I.A.; An, C. Review on Fixed and Floating Offshore Structures. Part I: Types of Platforms with Some Applications. *J. Mar. Sci. Eng.* **2022**, *10*, 1074. [CrossRef]
6. Wright, B. *Evaluation of Full Scale Data for Moored Vessel Stationkeeping in Pack Ice*; PERD/CHC Report 26–200; National Research Council Canada: Ottawa, ON, Canada, 1999.
7. Zhou, L.; Su, B.; Riska, K.; Moan, T. Numerical simulation of moored structure station keeping in level ice. *Cold Reg. Sci. Technol.* **2012**, *71*, 54–66. [CrossRef]
8. Kong, S.; Ji, S.; Ji, S.; Wang, Y.Y.; Gang, X.H. Numerical analysis of ice load on floating platform in polar region based on high-performance discrete element method. *Chin. J. Ship Res.* **2021**, *16*, 64–70.
9. Jang, H.; Kim, M. Kulluk-shaped arctic floating platform interacting with drifting level ice by discrete element method. *Ocean Eng.* **2021**, *236*, 109479. [CrossRef]
10. Zhang, A.; Chuang, Z.; Liu, S.; Zhou, L.; Qu, Y.; Lu, Y. Dynamic performance optimization of an arctic semi-submersible production system. *Ocean Eng.* **2022**, *244*, 110353. [CrossRef]
11. Sargent, J.; Morgan, M. Augmentation of a Mooring System Through Dynamic Positioning. In Proceedings of the Offshore Technology Conference, Houston, TX, USA, 5–7 May 1974.
12. Strand, J.; Sørensen, A.; Fossen, T. Modeling and control of thruster assisted position mooring systems for ships. *IFAC Proc. Vol.* **1997**, *19*, 61–76.
13. Aamo, O.; Fossen, T. Controlling line tension in thruster assisted mooring system. In Proceedings of the 1999 IEEE International Conference on Control Applications, Kohala Coast, HI, USA, 22–27 August 1999; pp. 13–17.
14. Fang, S.; Blanke, M.; Leira, B.J. Optimal set-point chasing of position moored vessel. In Proceedings of the ASME 2010, 29th International Conference on Ocean, Offshore and Arctic Engineering, Shanghai, China, 6–11 June 2010; Volume 4, pp. 479–486.
15. Wichers, J.; Dijk, R.V. Benefits of using assisted DP for Deepwater Mooring Systems. In Proceedings of the Offshore Technology Conference, Houston, TX, USA, 3–6 May 1999.
16. Faltinsen, O.M. *Sea Loads on Ships and Offshore Structures*; Cambridge University Press: Cambridge, UK, 1990.
17. Maruo, H. The drift of a body floating on waves. *J. Ship Res.* **1960**, *4*, 1–10.
18. Pinkster, J.A.; van Oortmerssen, G. Computation of the first and second-order wave forces on oscillating bodies in regular waves. In *Proceedings of the 2nd International Conference on Numerical Ship Hydrodynamics*; University of California: Berkeley, CA, USA, 1977; pp. 136–159.
19. Hallquist, J.O. *LS-DYNA. Theoretical Manual*; Livermore Software Technology Corporation: Livermore, CA, USA, 2006.
20. Shen, H.H.; Hibler, W.D.; Lepparanta, M. On applying granular flow theory to a deforming broken ice field. *Acta Mech.* **1986**, *63*, 143–160. [CrossRef]
21. Campbell, C.S. Stress-controlled elastic granular shear flows. *J. Fluid Mech.* **2005**, *539*, 273–297. [CrossRef]
22. Potyondy, D.O.; Cundall, P.A. A bonded-particle model for rock. *Int. J. Rock Mech. Min. Sci.* **2004**, *41*, 1329–1364. [CrossRef]
23. Mollon, G.; Zhao, J. Fourier–Voronoi-based generation of realistic samples for discrete modelling of granular materials. *Granul. Matter.* **2012**, *14*, 621–638. [CrossRef]

24. Pangalila, F.V.; Martin, J.P. A Method of Estimating Line Tensions and Motions of a Semi-submersible Based on Empirical Data and Model Basis Results. In Proceedings of the Offshore Technology Conference, Houston, TX, USA, 17–20 May 1969; Volume 2, pp. 90–96.
25. Igor, T.; Oleg, E.; Walter, P.; Barbaros, C. Numerical Modeling of Nonlinear Elastic Components of Mooing Systems. *IEEE J. Ocean. Eng.* **2005**, *30*, 37–46.
26. Minorsky, N. Directional stability of automatically steered bodies. *J. ASNE.* **1922**, *42*, 280–309. [CrossRef]
27. *ISO 19906*; Petroleum and Natural Gas Industries-Arctic Offshore Structures. International Organization for Standardization: Geneva, Switzerland, 2019.
28. DNV. *Sesam User Manual Sesam Manager*; DNV: Høvik, Norway, 2018.
29. Zhang, A.; Chuang, Z.; Liu, S.; Chang, X.; Hou, L.; He, Z.; Liu, S. Research on Mooring System Design for Kulluk Platform in Arctic Region. *Water.* **2022**, *14*, 1762. [CrossRef]
30. Ye, L.; Wang, C.; Chang, X.; Zhang, H. Propeller-ice contact modeling with peridynamics. *Ocean. Eng.* **2017**, *139*, 54–64. [CrossRef]
31. Wang, C.; Xiong, W.; Chang, X.; Ye, L.; Li, X. Analysis of variable working conditions for propeller-ice interaction. *Ocean. Eng.* **2018**, *156*, 277–293. [CrossRef]
32. Xie, C.; Zhou, L.; Ding, S.; Liu, R.; Zheng, S. Experimental and numerical investigation on self-propulsion performance of polar merchant ship in brash ice channel. *Ocean. Eng.* **2023**, *269*, 113424. [CrossRef]
33. Sun, Q.; Zhang, M.; Zhou, L.; Garme, K.; Burman, M. A machine learning-based method for prediction of ship performance in ice: Part I. ice resistance. *Mar. Struct.* **2022**, *83*, 103181. [CrossRef]